Stochastic Dynamics Simulations of Macromolecular Diffusion in a Model of the Cytoplasm of Escherichia coli

ARTICLE *in* THE JOURNAL OF PHYSICAL CHEMISTRY · FEBRUARY 1996

Impact Factor: 2.78 · DOI: 10.1021/jp9525191

Stochastic Dynamics Simulations of Macromolecular Diffusion in a Model of the Cytoplasm of *Escherichia coli*

Dominique J. Bicout[†] and Martin J. Field*

Laboratoire de Dynamique Moléculaire, Institut de Biologie Structurale−Jean-Pierre Ebel, 41 Avenue des Martyrs, 38027 Grenoble Cedex 01, France

Received: August 28, 1995; In Final Form: December 11, 1995[⊗]

Stochastic dynamics simulations have been performed to investigate macromolecular diffusion in the cytoplasm of the bacterium *Escherichia coli*. The cytoplasm was modeled as a polydisperse mixture of three different types of spherical particles representing ribosomes, proteins, and tRNA molecules at their physiological concentrations. The interactions between the particles consisted of short-range Lennard-Jones and long-range electrostatic terms. A number of properties, including the pair distributions functions, the static structure factor, and the long-time self-diffusion coefficients, were obtained for various model systems differing from each other by the size of the charges on the particles. The effect of macromolecular crowding on these properties is examined, and their implication for the dynamics of macromolecules within living cells is discussed.

1. Introduction

The nature of diffusion in crowded environments is an exciting problem that has attracted considerable attention in recent years. It is particularly important because the diffusion of biomacromolecules *in vivo* occurs, almost exclusively, in congested, heterogeneous media. The cytoplasm of living cells, for example, contains diverse populations of soluble macromolecules with various shapes and sizes and in various states of aggregation. Individually not all of the species may be present at very high concentrations, but collectively they occupy a substantial fraction of the total volume of the medium.[1,2]

In addition to the general diffusion of macromolecules, most biochemical reactions require some sort of diffusion-mediated encounter step, in which molecules (proteins, nucleic acids, and substrate molecules) are brought together via translational and rotational diffusional motions that are often guided by specific interactions between the particles. In many cases this step determines the rate of reaction. Northrup and Erickson, for example, have recently performed Brownian dynamics simulations to show that a diffusional mechanism is sufficient to explain the larger than expected bimolecular rate constants that are often observed for the formation of protein−protein complexes.[3]

Because of the importance of these processes it seems apposite to improve our understanding of the diffusion of macromolecules by studying intracellular dynamics and the organization of the intracellular environment. These investigations can be done by using computer simulations, but the modeling of the dynamics of such systems raises some problems. First, the individual macromolecules themselves are highly complex particles with complicated interactions. Second, there are a large variety of these molecules with a wide distribution of sizes and shapes, implying that a wide range of time scales needs to be considered when investigating their dynamics.

The problem of the Brownian motion of noninteracting large particles in solution has been well understood since the pioneering work of Einstein.[4] In this case, the interaction between a particle and the solvent particles can be replaced by a stochastic force. The problem is then reduced to solving a Langevin or a Fokker−Planck equation. In the macromolecular solutions that we wish to study, the concentration of Brownian particles is sufficiently high that the interactions between the large particles must be considered. Unfortunately a general solution of the Fokker−Planck equation which describes such systems is not possible although exact results for some simple cases are known. These include, for example, work on dilute solutions of hard spheres without hydrodynamic interactions.[5,6] More elaborate theories, such as the advanced kinetic theory[7,8] or the mode−mode-coupling approximation,[9] have been applied to the investigation of the dynamics of macromolecular suspensions for intermediate and high concentrations of hard spheres. These theories, however, give only qualitative agreement with the results obtained experimentally for real suspensions, whereas the results of numerical simulations give better agreement.

Because of the polydispersity and the high concentration of macromolecules in living cells, the conditions of intracellular diffusion of biomolecules are likely to differ substantially from classical Einstein diffusion. Relatively little simulation work seems to have been done in the area of crowded media[10] although stochastic dynamics simulations have proved important tools for the study of few-particle systems (see, for example, ref 11). However, Zimmerman and Minton[12] have emphasized the need for consideration of the effects of macromolecular crowding on biochemical, biophysical, and physiological processes, and Muramatsu and Minton[13] and Han and Herzfeld[14] have studied macromolecular diffusion in crowded solutions using scaled particle theory. In the same spirit, but using a different approach, Dwyer and Bloomfield[15] have developed a Brownian dynamics algorithm, based on the Ermak and McCammon[16] algorithm, for simulating the diffusion of bovine serum albumin (modeled as a single bead) in solutions of short-chain DNA (modeled as a string of beads) as a function of DNA concentration, albumin concentration, and ionic strength. They obtained quite good agreement between simulated and experimental data concluding that, with a relatively simple model, Brownian dynamics can be a useful tool for studying macromolecular transport in living systems.

* Author to whom correspondence should be addressed. Telephone: (33)-76-88-95-94. Fax: (33)-76-88-54-94. E-mail: mjfield@ibs.fr.
[†] E-mail: bicout@ibs.fr.
[⊗] Abstract published in *Advance ACS Abstracts,* February 1, 1996.

0022-3654/96/20100-2489$12.00/0

TABLE 1: Various Parameters for the Particles Used in the Simulations[a]

		ribosome $n = 12$	protein $n = 188$	tRNA $n = 136$
number density (nm^{-3})	H	46.9	55	39.8
	C	35	35	35
	N	12	10	13.7
	O	19	11	26
	P	2	0	3.7
mass density (kg m^{-3})	μ	1624	1315	1891
radius (nm)	a	9	3.6	1.73
hydrodyn radius (nm)	a^{hyd}	12	4.3	2.7
free diffusion coefficient (nm^2/ns)	$D_0 = k_B T/6\pi\eta a^{hyd}$	0.01785	0.04981	0.07933
volume fraction (%)	ϕ_0	9.16	9.19	0.737
interparticle spacing (nm)	$\xi = a\phi_0^{-1/3}$	19.96	7.98	8.89
Brownian relaxation time (ns)	$\tau_B = 2a^2\mu/9\eta$	0.0292	0.0038	0.0013
hydrodyn relaxation time (ns)	$\tau_H = \xi^2/\nu_0$	0.398	0.064	0.079
structural relaxation time (ns)	$\tau_0 = a^2/D_0$	4538.07	260.19	37.73
Schmidt number ($\times 10^4$)	$Sc = \nu_0/D_0$	5.6	2.0	1.26

[a] For all calculations we have taken the following values: liquid viscosity, $\eta = 1.002 \times 10^{-3}$ Pa s; kinematic viscosity of liquid, $\nu_0 = 10^{-6}$ m^2 s^{-1}; temperature, $T = 293$ K. We also give the Schmidt number, Sc, which measures the relative importance of convective to diffusive transport. A large Sc means that diffusive motion is less efficient for a transport process in the medium. Note that one of the consequences of crowding is an enhancement of Sc.

In this work, we report the results of stochastic dynamics simulations of macromolecular diffusion in the cytoplasm of the bacterium *Escherichia coli* (*E. coli*) with the aim of obtaining a clear picture of the effects of crowding on the dynamical structure of this medium. This has been done by computing both structural and dynamic properties, including pair distribution functions, the static structure factor, and the long-time self-diffusion coefficients, for various model systems that differ from each other by the size of the charges on the particles. It is the changes in the charges that influence the polydispersity of the medium and its effective crowding.

The outline of the paper is as follows. In section 2 we describe our model system, a detailed analysis of the simulation results is given in section 3, and the paper ends with some concluding remarks in section 4.

2. Methods

In this section we specify the composition of the system, the nature of the particles and their interactions, and the algorithm used to integrate the stochastic equations of motion.

2.1. Composition of the System. Sufficiently detailed data about the composition of the cytoplasm of organisms are only readily available for the bacterium *E. coli*, and so we chose a model of this system for our simulations. The very nice review article by Goodsell provided the inspiration for this work,[1] and it was upon the data described there that we based the composition of our model system.

There are essentially four types of large particle in the cytoplasm (outside of the nuclear region): proteins, ribosomes, tRNAs, and mRNAs. In this initial work, where we wanted to consider the simplest model possible, we chose to simulate a cubic box of 73.68 nm containing 12 ribosomes (r), 136 tRNAs (t), and 188 proteins (p), giving 336 particles in all. This matches the composition given by Goodsell for these particles. The mRNA molecules (for which, on average, there should be about 0.5 in a box of our size) were omitted.

Each of the particles was assumed to be spherical. The masses, radii (both actual and hydrodynamic), and number densities of each atom in the particles were chosen to be as close as possible to the available experimental values (which were obtained from refs 17−20). Because of the great diversity of protein sizes, an average protein particle was chosen which corresponds to a particle of mass about 160 kDa (i.e. a tetramer of 4 × 40 kDa chains). All the data for the particles are summarized in Table 1. The volume fractions for the system are about 20% and 40% when the actual and the hydrodynamic particle radii are used, respectively.[21]

Once the particle properties have been specified, the properties of the medium in which the large particles are immersed need to be defined. In particular we need to define the Debye screening length, the dielectric constant, and the viscosity of the medium. The temperature for all the simulations was taken to be 293 K.

The most problematic of these parameters is the Debye screening length, κ^{-1}, because the ionic conditions in the cytoplasm are sensitive to external conditions.[22] However, for our simulations we chose a value of $\kappa^{-1} = 1$ nm, which roughly corresponds to the value expected for the concentration of small molecules and ions in the cytoplasm given by Goodsell[1] if each is singly charged. This is an approximate value, and we intend to investigate the effect of changing this in future simulations.

For the viscosity of the solution we chose a value of 1.002×10^{-3} Pa s, which is equal to that of bulk water at the appropriate temperature, because recent experimental work has indicated that the cytoplasmic viscosity is not that different (see, for example, the review by Luby-Phelps[23]). Using similar reasoning we used a dielectric constant of $\epsilon = 80.2$.

2.2. Particle Interactions. The interactions between the particles were represented by a sum of repulsive, dispersive, and electrostatic terms. The hydrodynamic interactions were ignored in these initial studies for simplicity. However, their omission can be justified to some extent by the following argument. Both Brownian motion and hydrodynamic interactions arise from thermal fluctuations in the liquid and are connected through the space dependence of the diffusion coefficient tensor. Hydrodynamic interactions, which act to couple both the random displacements and the drift terms, are characterized by a hydrodynamic relaxation time, τ_H, which is the time taken by a viscous shear wave to propagate between two particles. For large average interparticle spacing, hydrodynamic interactions can be neglected. In this work, the values of the hydrodynamic relaxation times are relatively small, ranging between τ_B (the Brownian relaxation time) and τ_0 (the structural relaxation time) ($\tau_B \ll \tau_H \ll \tau_0$, see Table 1). This limits the effects of hydrodynamic interactions to short time scales which do not affect the long-time behavior, i.e. for times $t \gg \tau_H$. The hydrodynamic properties of particles were represented in our simulations simply by using the hydrodynamic radii of the particles instead of the actual radii to calculate their free diffusion coefficients, D_0. This renormalization of

the bare diffusion coefficient has also been used by Medina-Noyola,[24] who used the factorization approximation to separate the effects of hydrodynamic interactions and of the caging caused by direct interactions on particle motions.

The repulsive and dispersive interaction energy, $\epsilon_{ij}^{\mathrm{LJ}}$, between two particles, *i* and *j*, was calculated from the following formula:

$$\epsilon_{ij}^{\mathrm{LJ}} = \epsilon_{ij} + \epsilon_{\mathrm{water/water}} - \epsilon_{i/\mathrm{water}} - \epsilon_{j/\mathrm{water}} \tag{1}$$

where each term in the sum has the form

$$\epsilon_{kl} = \sum_{\alpha\in k}\sum_{\beta\in l}\int_{\alpha}\mathrm{d}\vec{r}_{\alpha}\int_{\beta}\mathrm{d}\vec{r}_{\beta}\,\varrho_k^{\alpha}(\vec{r}_{\alpha})\rho_l^{\beta}(\vec{r}_{\beta})\sqrt{d_{\alpha}d_{\beta}}\left[\left(\frac{s_{\alpha\beta}}{r_{\alpha\beta}}\right)^{12} - 2\left(\frac{s_{\alpha\beta}}{r_{\alpha\beta}}\right)^{6}\right] \tag{2}$$

In this equation the functions ρ are the density distribution functions of the atom types α and β in the particles *k* and *l*. d_{α}, d_{β}, and $s_{\alpha\beta} = (s_{\alpha} + s_{\beta})/2$ are the standard Lennard-Jones parameters for the atom types in the particle. The overall interaction between two particles appears rather complicated, but it can be simplified because the particles are spherical and the densities of each atom type within each sphere are uniform. Equation 2 can be rewritten as

$$\epsilon_{ij}^{\mathrm{LJ}} = \int_{\mathrm{sphere}\,i}\mathrm{d}\vec{r}_i\int_{\mathrm{sphere}\,j}\mathrm{d}\vec{r}_j\left(\frac{A_{ij}^{\mathrm{LJ}}}{r_{ij}^{12}} - 2\frac{B_{ij}^{\mathrm{LJ}}}{r_{ij}^{6}}\right) \tag{3}$$

where the integrations are over the space occupied by each particle only. The coefficients A_{ij}^{LJ} and B_{ij}^{LJ} are constants for each type of interaction and can be precomputed. Because the total interaction energy (eq 1) is the sum of four terms, the coefficients are also the sum of four terms, A_{kl} and B_{kl}. The A_{kl} terms have the form

$$A_{kl} = \sum_{\alpha\in k}\sum_{\beta\in l}\rho_k^{\alpha}\rho_l^{\beta}\sqrt{d_{\alpha}d_{\beta}}s_{\alpha\beta}^{12} \tag{4}$$

where the ρ quantities are now the number densities for the atoms in each particle. The expression for the B_{kl} coefficients is similar except that the exponent of the $s_{\alpha\beta}$ term is 6. The number densities for the particles are those given in Table 1. For water the densities (nm^{-3}) were as follows: H, 66.6; O, 33.3. The Lennard-Jones parameters, [*d* (kJ mol^{-1}) and *s* (nm)], for each atom were as follows: H, {0.08, 0.100}; C, {0.50, 0.185}; N, {0.67, 0.175}; O, {0.84, 0.160}; P, {0.84, 0.210}. Initially we tried several different sets of Lennard-Jones parameters, but we did not find significant differences in the results.

The integrals in eq 3 can be performed straightforwardly (see, for example, refs 25 and 26). However, because of their rather complicated functional form, spline fits were determined for the interactions between each type of particle (i.e. for three types of particle there are six different types of interaction) and it was these that were used to calculate the interaction energy and its derivatives during the simulations. Overall the interaction term given by the expression from eq 1 has an extremely steep repulsive part and a very narrow, shallow attractive well. The total interaction energy for each particle falls off very rapidly and is essentially zero ($<10^{-6}$ kJ mol^{-1}) at distances 1−1.5 nm larger than the sum of the particle radii.

The electrostatic interactions were calculated using DLVO (Derjaguin−Landau−Verwey−Overbeek) theory.[26,27] For two particles, *i* and *j*, at a distance r_{ij} apart and with charges *Ze* (*e* being the elementary charge) and radii *a*, the interaction energy, $\epsilon_{ij}^{\mathrm{DLVO}}$, is

$$\epsilon_{ij}^{\mathrm{DLVO}} = \frac{Z_iZ_je^2}{\epsilon r_{ij}}\left(\frac{\mathrm{e}^{\kappa a_i}}{1+\kappa a_i}\right)\left(\frac{\mathrm{e}^{\kappa a_j}}{1+\kappa a_j}\right)\mathrm{e}^{-\kappa r_{ij}} \tag{5}$$

where κ is the inverse Debye screening length and ϵ is the dielectric constant of the medium. Cytoplasmic proteins appear to have small net negative charges, and so we guessed a total charge of $Z = -4$ for our simulations. The net charge of the tRNAs was calculated assuming that each base carries a charge of −1 to give $Z = -75$. For the ribosomes, we could find no experimental data giving their effective charge. However, the number of bases in the rRNA and the sequences of all its constituent proteins are known and it is possible to determine a net total charge of about −2500. We do not present the results of simulations for such high charges for two reasons. First, we are uncertain that the ribosome does indeed show such a high effective charge, as there are likely to be strongly-bound neutralizing counterions with very limited mobility that cannot be accounted for within the DLVO/Debye−Hückel approximation that we used to calculate the electrostatic interactions. Second, the results of limited simulations using ribosomes with such high charges show that the behavior of these systems does not differ qualitatively from those with charges of −1000. Instead, in the absence of available data for comparison, we chose a variety of charge models for the ribosome. These and the details of the charges on the other particles are summarized in Table 2. Note that the Debye screening length was fixed at a value of $\kappa^{-1} = 1$ nm for all the simulations.

Both the Lennard-Jones and the DLVO interaction terms between the particles were calculated using a list-based approach; i.e., for each particle a list of interactions was kept which was updated periodically as the particles moved. To be included on the lists, an energy cutoff was used. Interactions with a value of less than $10^{-6}k_{\mathrm{B}}T$ were excluded. Because of the much shorter range of the Lennard-Jones interactions, separate lists were kept for the interaction types. All interactions were calculated using the minimum-image convention.[28]

2.3. Simulations. The dynamics of the particles were represented by a Langevin equation:

$$m_i\frac{\mathrm{d}\vec{v}_i}{\mathrm{d}t} = \vec{F}_i(\vec{r}_i) - m_i\zeta_i\vec{v}_i + \vec{R}_i \tag{6}$$

where m_i, $\vec{r}_i$, and $\vec{v}_i$ are the particle's mass, position, and velocity, respectively. $\vec{F}_i$ is the force on the particle, which is calculated using the interaction terms described above. ζ_i is the particle's friction coefficient, which is related to its free diffusion coefficient, D_{0_i}, and to its hydrodynamic radius, a_i^{hyd}, by

$$\zeta_i = \frac{k_{\mathrm{B}}T}{m_iD_{0_i}} = \frac{6\pi\eta a_i^{\mathrm{hyd}}}{m_i} \tag{7}$$

where η is the viscosity of the medium. $\vec{R}_i$ is a random force which is taken to be an independent stationary Gaussian random variable for each particle with zero mean and which has no correlations with the any of the particle forces or velocities. Its correlation function is

$$\langle\vec{R}_i(0)\cdot\vec{R}_j(t)\rangle = 6m_i\zeta_ik_{\mathrm{B}}T\delta_{ij}\delta(t) \tag{8}$$

The integration algorithm we used to perform the simulations was the leap-frog algorithm for stochastic dynamics developed by van Gunsteren and Berendsen.[29] This algorithm is valid for simulations with arbitrary values of the friction coefficient. The simpler algorithm of Ermak and McCammon[16] was not em-

TABLE 2: Charge and Polydispersity Parameters for the Studied Systems[a]

	ribosome		protein		tRNA					
System	Z	a' (nm)	Z	a' (nm)	Z	a' (nm)	$\langle a \rangle$ (nm)	σ	$\bar{\phi}$	$\bar{\xi}$ (nm)
I	0	9	0	3.6	0	1.73	3.04	0.48	0.191	5.27
II	−2	9	−4	3.6	−75	3.89	3.91	0.25	0.268	6.07
III	−500	10.96	−4	3.6	−75	3.89	3.98	0.34	0.342	5.70
IV	−1000	11.54	−4	3.6	−75	3.89	4.00	0.36	0.369	5.58

[a] The Debye screening length is $\kappa^{-1} = 1$ nm.

ployed because we had to use a relatively short time step so as to integrate properly over the steeply varying short-ranged dispersive potential. With a short time step, Δt, the constraint condition, $\Delta t \gg \tau_{B,i} = m_i D_{0i}/k_B T$, which is necessary for the Ermak and McCammon algorithm to be valid, is no longer satisfied.

All simulations were carried out for the system of 336 particles described above with standard periodic boundary conditions.[28] The velocities of the particles at the start of each simulation were assigned from a Gaussian distribution at a temperature of 293 K. For each charge model five simulations were performed. The time step for the simulations was $\Delta t = 0.0025$ ns, and each simulation consisted of 3×10^6 time steps (or 7.5 μs). The coordinates and velocities of the particles were saved every 200 steps, giving five trajectories of 15 000 coordinate and velocity arrays for each set of simulations. These trajectories were then used to perform the analyses that are described in the following section. All calculations were carried out on a network of HP 9000/735 workstations.

3. Results and Discussion

The cytoplasm is a multicomponent mixture containing macromolecular particles with a range of distributions of size and of polydispersity. A useful index, σ, of the polydispersity for spherical particles is the square root of the standard deviation of the particle radii, a, divided by the mean of the particle radii (where the angular brackets denote an average over the individual particle values):

$$\sigma = \left(\frac{\langle a^2 \rangle}{\langle a \rangle^2} - 1 \right)^{1/2} \tag{9}$$

Two other useful parameters are the volume fraction calculated using the average volume of the particles, which we call the *average volume fraction*, $\bar{\phi}$, and the average interparticle spacing, $\bar{\xi}$, which are defined by

$$\bar{\phi} = \frac{4\pi \langle a^3 \rangle \rho}{3} \quad \text{and} \quad \bar{\xi} = \langle a \rangle \bar{\phi}^{-1/3} \tag{10}$$

where ρ is the particle density.

Electrostatic interactions between particles will modify the size distribution or polydispersity. These changes are controlled by the particle charges, Z_i, and the Debye screening length κ^{-1}. In what follows, we take the uncharged system I as a reference for all calculated quantities. For the discussion of the polydispersity characteristics of the charged systems, effective radii, a', need to be determined for each component. These were defined as the value at which the beginning steep parts of the pair correlation functions for the $i-i$ component in the charged and uncharged systems coincided when plotted in the dimensionless scales r/a' and r/a, respectively (a description of the calculation of the pair correlation functions and a discussion of their results is given in detail below). In all cases it was found that the two pair correlation functions were essentially superimposable throughout their range. The results obtained for the effective particle radii and for the corresponding polydispersity parameters for all four systems are given in Table 2.

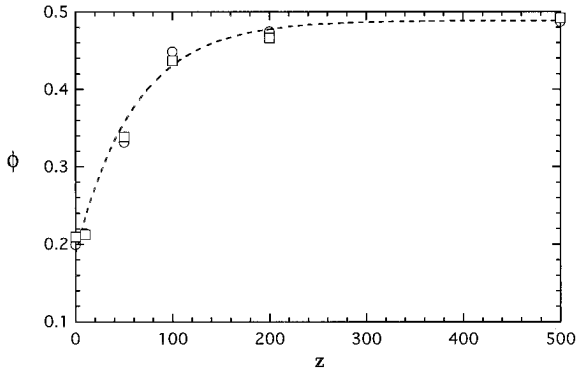

Figure 1. Variation of the volume fractions $\phi_d(Z)$ (circle) and $\phi_g(Z)$ (square) versus the absolute value of the charge Z for a monodisperse system of spherical particles of radius 3.6 nm at a reference volume fraction of 20.9%. The dashed line is the best fit to the data of a single exponential of Z plus a constant.

To test the above procedure, we carried out simulations of a monodisperse system of spherical particles of radius $a = 3.6$ nm with zero charges, with a volume fraction equal to 20.9% and a Debye screening length equal to 1 nm. The pair correlation function and the self-diffusion coefficient as a function of the charge were computed, and the effective radius was determined as described above. The effective radii determined from the pair correlation functions can be used to determine a volume fraction as a function of particle charge, Z, which we denote $\phi_g(Z)$. Another volume fraction parameter, $\phi_d(Z)$, can be calculated from the Z-dependent self-diffusion coefficient, $D_s(Z)$. This is done by making the assumption that the effect of electrostatic interactions between particles consists in a modification of the volume fraction due to the changes in particles sizes. In other words, below the freezing transition, which for hard spheres occurs at a volume fraction of 49.4%, the relation $D_s(Z) = D_0[1 - 2\phi_d(Z)]$ was considered to be valid to first order in $\phi_d(Z)$.[6] The computed data for the rescaled volume fraction are displayed in Figure 1, which shows that the rescaling procedure described above gives satisfactory results.

In light of the results in Table 2, we are now in a position to discuss the static and dynamic properties of our model system of the cytoplasm in more detail.

3.1. Structure. The averaged pair distribution function or the pair correlation function is

$$g(r) = \frac{V}{N^2} \left\langle \sum_{i=1}^{N} \sum_{j \neq i}^{N} \delta(\vec{r} - \vec{r}_i + \vec{r}_j) \right\rangle \tag{11}$$

where N is the total number of particles, V is the volume of the system, and $\vec{r}$ are the particle positions. $g(r)$ gives the probability of finding a pair of particles a distance r apart relative to the probability expected for a completely random distribution of the same density. The pair correlation is useful because it provides a description of the structure of a colloidal suspension and measures the extent to which the structure of the fluid

deviates from complete randomness. The function $g(r)$ plays a central role in the physics of fluids for two main reasons. First, the radial distribution function is directly measurable by radiation-scattering experiments. Second, provided that the particles interact through pairwise additive forces, the thermodynamic properties of the fluid can be written as integrals over $g(r)$. For noninteracting particles, $g(r) = 1$, whereas, for interacting particles, nearest-neighbor shells are formed and oscillations in $g(r)$ are expected. For multicomponent suspensions composed of n (here, $n = 3$) distinct species of particles, the total pair correlation function is given by

$$g(r) = \sum_{\alpha,\beta=1}^{3} x_\alpha x_\beta g_{\alpha\beta}(r) \quad \text{with} \quad g_{\alpha\beta}(r) = \frac{V}{N_\alpha N_\beta} \langle \sum_{i=1}^{N_\alpha} \sum_{j=1}^{N_\beta} \delta(\vec{r} - \vec{r}_i^{\,\alpha} + \vec{r}_j^{\,\beta}) \rangle \quad (12)$$

where $g_{\alpha\beta}(r)$ is the partial radial distribution function of particles of kind β around an origin particle of kind α, and $x_\alpha = N_\alpha/N$.

All combinations of pair distribution functions, $g_{\alpha\beta}(r)$, were computed for each of the four systems, and the correlation functions, $g_{\alpha\alpha}(r)$, were used for rescaling the effective particle sizes as described above. The $g_{\alpha\alpha}(r)$ values for all the particle types in all four systems were very similar, and no significant differences could be seen. Therefore, we concentrate our discussion on the cross-correlation functions $g_{\alpha\beta}(r)$ ($\alpha \neq \beta$), which are drawn in Figure 2. Generally speaking, for all the $g_{\alpha\beta}(r)$, there is a sharp first peak with little other structure. This implies that the first shell of neighbors is well defined, but the systems are homogeneous beyond this point. However, the different systems do display different behaviors at short range at distances on the order of the sum of the (unrescaled) particle radii, $\sigma_{\alpha\beta} = a_\alpha + a_\beta$. We discuss each of the pair correlation functions in turn:

Ribosome−Protein (Figure 2a). No differences appear between systems I (without charges) and II (with charges), meaning that the electrostatic interactions are not yet strong enough to modify the relative structure between the ribosomes and proteins. On the other hand, the position of the first peak, initially at σ_{rp} in systems I and II, is shifted to $1.17\sigma_{rp}$ in system III, and the second, broad peak at roughly $1.84\sigma_{rp}$ becomes more pronounced. In system IV, where the charge of the ribosomes is higher, the first peak is further shifted to $1.22\sigma_{rp}$ and the second one has split.

Ribosome−tRNA (Figure 2b). The most noteable feature of these curves is the first peak of system II, which is larger than those of all the other systems. Its position is close to that of system I at $1.06\sigma_{rt}$. Furthermore, the $g_{rt}(r)$ of system II has a distinct second peak at $2.08\sigma_{rt}$ while the curves for the other systems are relatively featureless. The appearance of the second peak in the system II implies that the repulsive interactions between ribosomes and tRNAs are strong enough to form a well-defined second nearest-neighbor shell. As the charge of the ribosomes gets larger, the first peaks in systems III and IV become broader and are shifted to $1.53\sigma_{rt}$ and $1.58\sigma_{rt}$, respectively, and the structure of the second shell is disrupted.

Protein−tRNA (Figure 2c). System I is characterized by a first peak very close to σ_{pt} and by the absence of a second peak. For the three other systems, $g_{pt}(r)$ has the same shape and exhibits a well marked first peak shifted to $1.5\sigma_{pt}$ and a broad second peak at roughly $3\sigma_{pt}$. The difference in the height of the first peak between systems I and II comes from the additional repulsive electrostatic interactions between particles in system II. As the charge on the ribosomes becomes larger on moving from systems II to IV, the strong electrostatic interactions repel the proteins and tRNAs, confining them and enhancing the height of the peaks in $g_{pt}(r)$.

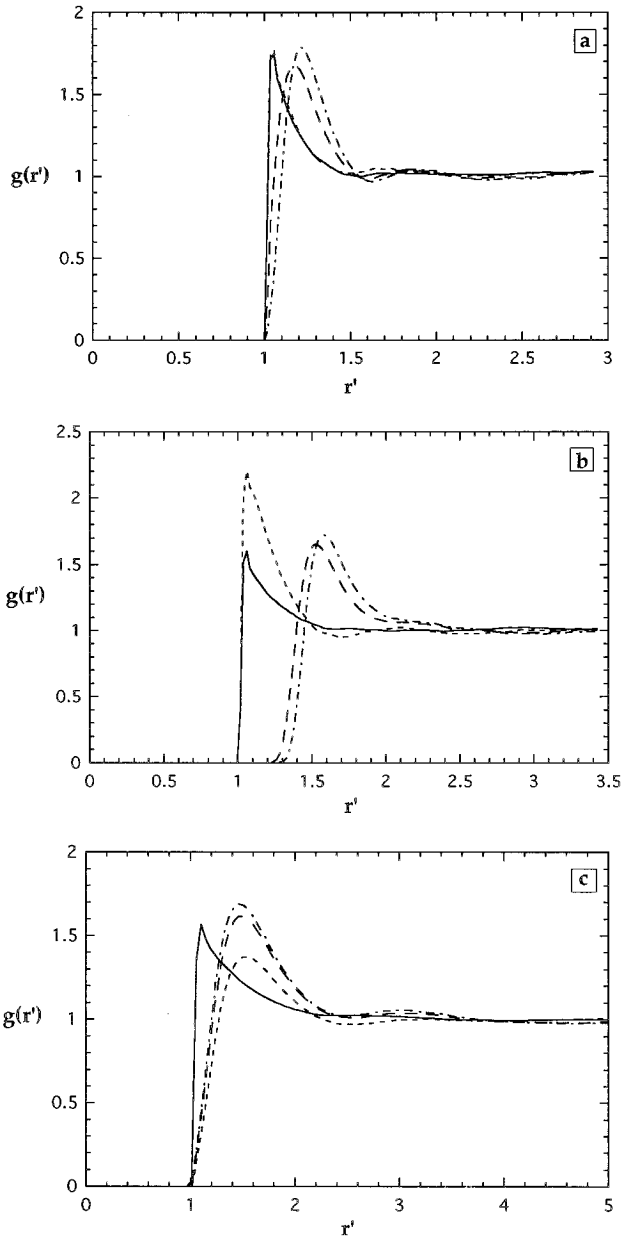

Figure 2. Pair distribution functions $g(r')$ versus reduced position $r' = r/\sigma_{\alpha\beta}$ ($\sigma_{\alpha\beta} = a_\alpha + a_\beta$) for different pairs, ($\alpha$,$\beta$), of particles for systems I (solid line), II (dashed line), III (long-dashed line), and IV (dot-dashed line). The cross-correlation functions are between (a) ribosome−protein with $\sigma_{rp} = 12.6$ nm, (b) ribosome−tRNA with $\sigma_{rt} = 10.73$ nm, and (c) protein−tRNA with $\sigma_{pt} = 5.33$ nm.

Recently Mazur has proposed[30] that the radial distribution function, $G(r) = 4\pi\rho r^2 g(r)$, can be partitioned into "neighborship" distribution functions $P(1,r)$, $P(2,r)$, ..., $P(n,r)$, such that $P(1,r)\,dr$, $P(2,r)\,dr$, ..., $P(n,r)\,dr$ are the probabilities that the nearest (1st neighbor), next nearest (2nd neighbor), ..., nth neighbor will be found between r and $r + dr$. It follows that

$$G(r) = P(1,r) + P(2,r) + ... + P(N-1,r) \quad (13)$$

For an homogeneous system and within the superposition approximation, these functions can be recursively obtained to

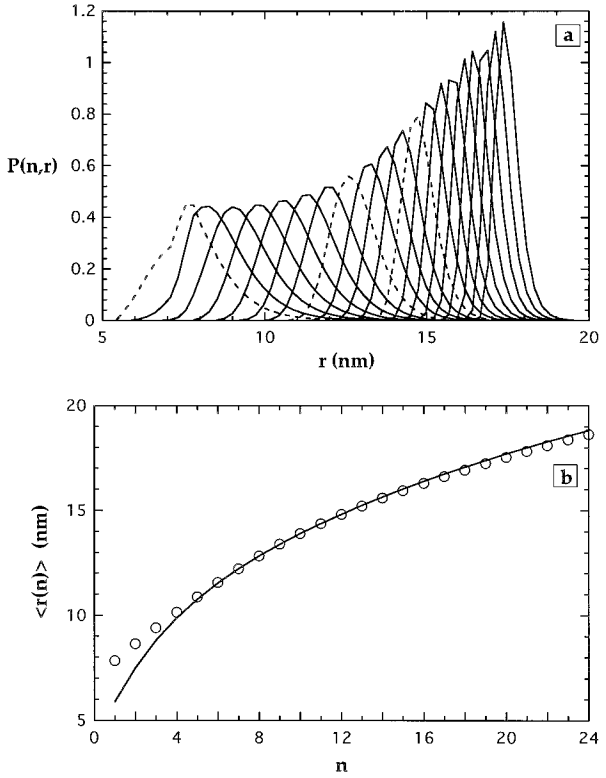

Figure 3. (a) Neighborship distribution functions $P(n,r)$ for $n = 1-20$ in system IV. Dashed curves from left to right represent the functions $P(1,r)$, $P(8,r)$, and $P(12,r)$, respectively. (b) Mean neighborship distances for system IV (symbols) and for an ideal gas (solid line) at the same number density.

any desired n from the following relation:

$$P(n,r) = [G(r) - \sum_{m=1}^{n-1} P(m,r)] \times \exp\{-\int_0^r dr' [G(r') - \sum_{m=1}^{n-1} P(m,r')]\} \quad (14)$$

The study of these functions is a valuable tool for the analysis of the structural features of a system, and it is straightforward to generalize this procedure to the study of the partial distribution functions, $G_{\alpha\beta}(r)$, where $G(r) = \sum_{\alpha,\beta=1}^{3} x_\alpha x_\alpha G_{\alpha\beta}(r)$. To get some insight about the microstructure of the system regardless of the nature of the particles, the partition of the total distribution function $G(r)$ into neighborship distributions was performed and the functions $P(n,r)$ were computed for each system. As the shapes of $P(n,r)$ are quite similar for all systems, we have displayed the results for system IV only for $n = 1-20$ (see Figure 3a). It can be seen that there is no overlap between $P(1,r)$ and $P(12,r)$, meaning that the probability of finding clusters with face-centered cubic (fcc) symmetry is vanishingly small. However, there is a small region of overlap between $P(1,r)$ and $P(8,r)$, indicating the possible occurrence of body-centered cubic (bcc) clusters. A useful quantity for comparison which measures the equivalence among subsets of neighbors is $\langle r(n)\rangle$, the mean distance from the reference particle to each neighbor. It is defined by

$$\langle r(n)\rangle = \int_0^\infty r P(n,r)\, dr \quad (15)$$

Apart from the first three distances, it is found that the values of $\langle r(n)\rangle$ are identical for all systems. The results for system IV and for an ideal gas (for which $g(r) = 1$) at the same number density are compared in Figure 3b. It is clear that $\langle r(n)\rangle$ for system IV becomes very close to that for the corresponding ideal gas values for $n \geq 6$. In addition, as $\langle r(1)\rangle \simeq 2\langle a\rangle$ for systems III and IV, we conclude, following Mazur,[30] that these systems are in the random close packed state with n^* ($4 \leq n^* < 6$) neighbors. For the less dense systems I and II, $\langle r(1)\rangle \simeq 1.19 \times 2\langle a\rangle$ and $\langle r(1)\rangle \simeq 1.03 \times 2\langle a\rangle$, respectively, which implies that their overall spatial organization is approximately the same (because the curves of $\langle r(n)\rangle$ are almost identical for the four systems, except for the first few points) but that the interparticle spacing is larger. The finer points of the structure, as mentioned, can be examined by calculating the functions $P_{\alpha\beta}(n,r)$. This has been done, but due to space limitations, we do not present the results here.

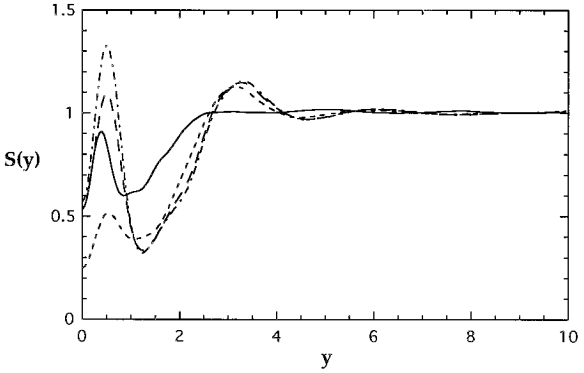

Figure 4. Total static structure factor $S(y)$ versus reduced wave number $y = q\langle a\rangle$ for systems I (solid line), II (dashed line), III (long-dashed line), and IV (dot-dashed line). $\langle a\rangle$ is the mean particle radius calculated from the rescaled radii for each system (see Table 2).

Another quantity of interest that can be calculated is the static structure factor, $S(q)$, which is directly measurable from X-ray and neutron scattering experiments and which describes the fluctuations in the density of the medium. $S(q)$ is related to $g(r)$ as follows:

$$S(q) = \frac{1}{N}\sum_{i,j}\langle \exp\{i\vec{q}(\vec{r}_i - \vec{r}_j)\}\rangle = 1 + 4\pi\rho\int_0^\infty r^2[g(r) - 1]\frac{\sin(qr)}{qr}\, dr \quad (16)$$

For a multicomponent fluid the structure factor can be written in the form

$$S(q) = \frac{1}{\overline{|f(q)|^2}}\sum_{\alpha,\beta} f_\alpha(q)\, f_\beta(q)\, S_{\alpha\beta}(q) \quad (17)$$

where the partial structure factors are defined by

$$S_{\alpha\beta}(q) = x_\alpha\delta_{\alpha\beta} + 4\pi\rho x_\alpha x_\beta\int_0^\infty r^2[g_{\alpha\beta}(r) - 1]\frac{\sin(qr)}{qr}\, dr \quad (18)$$

and the average form factor by

$$\overline{|f(q)|^2} = \sum_\alpha x_\alpha |f_\alpha(q)|^2 \quad (19)$$

with $|f_\alpha(q)|^2$ being the form factor for particle α. For an homogeneous spherical particle of radius a_α, one obtains

$$f_\alpha(q) = \frac{3}{(qa_\alpha)^3}\{\sin(qa_\alpha) - qa_\alpha\cos(qa_\alpha)\} \quad (20)$$

The static structure factors, $S(q)$, were computed for the four systems, and the results are displayed in Figure 4. It is apparent

that the structure of the suspension, as described by $S(q)$, is quite different for the uncharged and the charged systems. System I, with the smallest volume fraction but the highest polydispersity (see Table 2), exhibits only a single peak at $q\langle a\rangle \simeq 0.375$. For the charged systems II, III, and IV, $S(q)$ is characterized by two peaks separated by a large gap of order $3q\langle a\rangle$. The position of the first peak is shifted by roughly 0.125 from its position in system I. Qualitatively for the charged systems, the medium can be considered as a two-component mixture of small particles of size $\sim\langle a\rangle$ and of large particles of size $\sim 3\langle a\rangle$ (see Table 2). It follows that proteins and tRNAs are roughly identical particles for the structural organization of the medium. The first peak of the structure factor represents the small particles, which are enclosed in an array of large particles, which are themselves represented by the second peak. This correspondence is supported by noting that the position $q\langle a\rangle \simeq 0.5$ of the first peak does not change when the polydispersity goes up by increasing the charge number of ribosomes although the position of the second peak does move from $q\langle a\rangle \simeq 3.0$ to $q\langle a\rangle \simeq 3.3$. This displacement is caused by the growth of the effective size of ribosomes due to their increasing charge. Similarly, the height of the first peak gets higher as the charge on the ribosomes increases because the proteins and the tRNAs become more confined.

3.2. Dynamics. The time-dependent self-diffusion coefficient, $D_s(t)$, for a particle is defined in terms of the particle's mean-square displacement using the relation

$$\langle[\vec{r}(t) - \vec{r}(0)]^2\rangle = 6D_s(t)t \tag{21}$$

Two fundamental characteristic times intervene in the study of the stochastic motion of a particle. First is the Brownian relaxation time, τ_B (see Table 1), which represents the time scale below which the particle motion is ballistic and beyond which the particle undergoes stochastic motion. The second one is the structural relaxation time, τ_0 ($\tau_0 \gg \tau_B$, see Table 1), which is the time a Brownian particle needs to diffuse over its radius. Even for time scales $t \gg \tau_B$ the self-diffusion coefficient varies with time due to relaxation in the positions of the surrounding Brownian particles which occurs on time scales of τ_0. τ_0 has important consequences for suspension rheology. For a flowing fluid the value of $\Gamma\tau_0$ (Γ being the shear rate) separates the regime of Newtonian behavior for $\Gamma\tau_0 \ll 1$ from the non-Newtonian regime for $\Gamma\tau_0 \gg 1$. For the dynamics of the Brownian particle, the relaxation time separates two linear regimes in the behavior of the time dependent mean-squared displacement. The short (s) and long (l) time regimes are defined as follows:

$$D_s(t) = \begin{cases} D_s^s & \text{for} \quad \tau_B \ll t \ll \tau_0 \\ D_s^l & \text{for} \quad \tau_0 \ll t \end{cases} \tag{22}$$

At short times the particle diffuses quasi freely with the self-diffusion coefficient D_s^s, which takes the Stokes−Einstein value in the absence of hydrodynamic interactions. At intermediate times repulsive interactions with other particles considerably reduce its diffusional transport and the cage effect of the neighboring particles becomes the limiting process for the particle diffusion. After several rearrangements of the cage at longer times, the mean-squared displacement of the Brownian particle exhibits a second linear regime with the self-diffusion coefficient D_s^l, which is found to decrease with the increasing strength of the interactions.

Here, we are interested by the long-time behavior of the suspension medium, and so, for convenience, we drop the superscripts s and l. Thus, D_s will denote the self-diffusion coefficient in the long-time regime. Figure 5a shows the values of D_s for each species of particle in the four systems. It can be seen that D_s changes under the combined effects of the volume fraction, i.e. the crowding, and the polydispersity. As expected, D_s for all particles exhibits an overall tendency to decrease with the average volume fraction. The decreasing gradient, of $\simeq -1.8$ for tRNAs, is about 1.3 and 5.6 times greater than those for the ribosomes and proteins, respectively. This high sensitivity of tRNAs and ribosomes to the crowding is due to their large charges. (It may be noted, in fact, that in system IV their electrostatic interactions have about the same order of magnitude because $Z_r/Z_t \sim (a_r/a_t)^{3/2}$.)

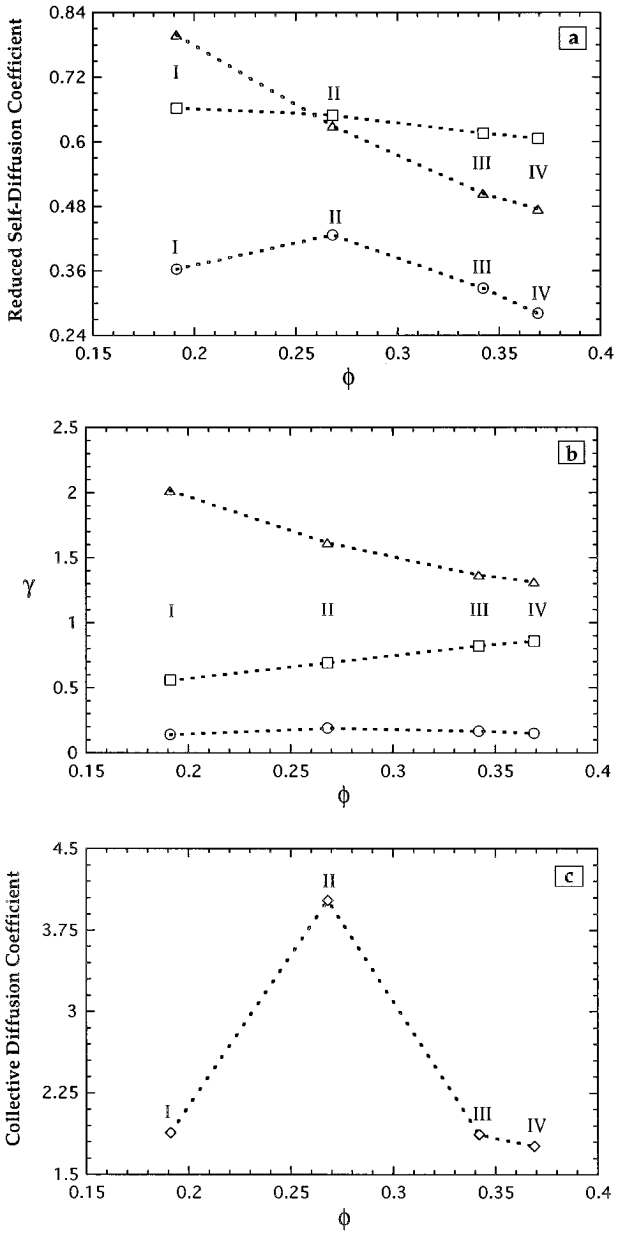

Figure 5. (a) Reduced self-diffusion constant D_s/D_0 as a function of the mean volume fraction, $\bar{\phi}$, for ribosomes (circles), proteins (squares), and tRNAs (triangles). (b) The ratio γ versus $\bar{\phi}$. (c) Reduced collective diffusion constant D_c/D_0 versus $\bar{\phi}$.

It is surprising that the value of D_s for ribosomes increases on going from the uncharged system I to the charged system II. This effect has a double origin. First, the repulsive electrostatic interactions between particles increase the average interparticle spacing (see Table 2). Second, because of their small charge in system II and their large size, the ribosomal electrostatic interactions are small. As a consequence, the

medium of system II looks less crowded for ribosomes and they can move more freely, causing an enhancement of their self-diffusion constant. Note that the values of D_s are not greatly influenced by the values of the polydispersity index of the systems, indicating that the electrostatic interactions have their effect because they increase the effective particle radii and, hence, the crowding in the medium.

It is worthwhile to analyze the diffusional motion in terms of tracer particles and mobile obstacles, both of which carry out stochastic motions with different self-diffusion coefficients or jump rates. The quantity of interest is the ratio, γ, of the jump rate of tracer particles to the average jump rate of cluster obstacles, defined as

$$\gamma_\alpha = \frac{D_\alpha}{\overline{D}_\alpha}, \quad \overline{D}_\alpha = \frac{\sum_{\beta\neq\alpha} x_\beta D_\beta}{\sum_{\beta\neq\alpha} x_\beta} \tag{23}$$

If $\gamma_\alpha \rightarrow \infty$, the cluster obstacles are immobile and their γ values are zero. There exists a critical value of the volume fraction, the percolation threshold, below which long-range diffusion of tracers is allowed but above which it is blocked. For $\gamma_\alpha = 1$ the surrounding obstacles and the tracers move on average at the same rate although their individual self-diffusion coefficients can be quite different.

Figure 5b shows γ as a function of the volume fraction. It is clear that the ribosomes can be considered as mobile obstacles by the protein and tRNA particles, while the true tracers are tRNAs which diffuse faster than the surrounding cluster obstacles formed by the ribosomes and proteins. These latter particles move slower than the surrounding effective obstacles. It is also evident that the jump ratio for both ribosomes and tRNAs decreases with crowding, while it increases for proteins which interact less with other particles because they have smaller charges. This indicates that, under certain conditions of the polydispersity and of the distribution of charges, proteins could move faster than tRNAs. The data of Figure 5b suggest that this could be achieved by increasing the ribosomal charge.

Another quantity that can be used to characterize the diffusional motion is the collective diffusion constant, D_c, which describes the diffusion of the overall density of the suspension medium. It is defined as $D_c = D_{eff}(0)$, where $D_{eff}(q)$ is the effective diffusion coefficient given by

$$D_{eff}(q) = \frac{\overline{D}_0(q)}{S(q)} \tag{24}$$

where the average bare diffusion constant is given by

$$\overline{D}_0(q) \frac{1}{|f(q)|^2} \sum_\alpha x_\alpha |f_\alpha(q)|^2 D_{0,\alpha} \tag{25}$$

D_c is commonly given in terms of a second virial parameter, λ_v, as

$$D_c = \overline{D}_0(1 + \lambda_v \overline{\phi}) \tag{26}$$

An expression for λ_v is given in the appendix while the average bare diffusion constant has the value $\overline{D}_0 = 0.060\,62$ nm^2/ns and the values of $\overline{\phi}$ are taken from Table 2. As shown in Figure 5c, D_c is quite sensitive to both the polydispersity and the charge model, and exhibits an overall tendency to decrease with the average volume fraction. For noncharged particles and small polydispersity, the collective diffusion constant reduces to[31] $D_c = \overline{D}_0[1 + (8 - 12\sigma^2)\overline{\phi}]$, which gives a value very close to that of system I, $D_c = 1.88\overline{D}_0$. The additional contribution of the repulsive electrostatic interactions in system II increases D_c to 2.3, its value in the neutral system. When the ribosomal charge gets larger, the nonrescaled part of the electrostatic contribution is exponentially washed out by the rescaled particle sizes (see the appendix) and λ_v and D_c decrease with the rescaled average volume fraction $\overline{\phi}$ (systems III and IV). The slow decrease of D_c in systems III and IV indicates that the major contribution of the electrostatic interactions due to the ribosomes is to rescale the sizes of the particles, essentially σ_{rr}, σ_{rp}, and σ_{rt}. Therefore, the two pair interactions, ribosome−protein and ribosome−tRNA, can be treated as simple equivalent hard spheres while the full interaction must be considered for the interacting pair protein−tRNA. Thus, the medium seems to behave as a three-component mixture of hard spheres with nonadditive interactions in the sense used by, for example, Schaink.[32]

4. Conclusion

The motivation for this work has been to develop a model system that could be used to help our understanding of macromolecular diffusion in hindered biological media, such as the cytoplasm of living cells. To do this, a stochastic dynamics algorithm was used to perform computer simulations of a three-component mixture of uniformly charged spheres representing ribosome, protein, and tRNA particles at their physiological concentrations. This work, situated at an intermediate level between studies of cellular structure and of individual macromolecules, presents a preliminary theoretical contribution to obtaining an understanding of the macromolecular dynamics in the interior of cells.

Simulations show that the magnitude of the particle charges plays an important role for the structure and the dynamics of the system. The structure is found to be a random close packed state with n^* ($4 \leq n^* < 6$) neighbors. The small particles, proteins, and tRNAs are located in the interstices of the lattice formed by the large particles, the ribosomes. This feature may be observed from the structure factor, $S(q)$, for which the second maximum, describing the ribosomes, occurs at $q\langle a\rangle \simeq 3.3$. The value expected for close packing is $q\langle a\rangle \simeq 3.8$.[33] Similarly, $g(r)$ exhibits a well defined first coordination shell of small particles at $2\langle a\rangle$ and a second one that includes large particles at about $4\langle a\rangle$. Long-range order is destroyed because of the weak range of the interactions and the polydispersity. The analysis of neighborship distribution functions, $P(n,r)$, allows us to investigate the local order and suggests, for example, that bcc clusters of particles could exist in the cytoplasm.

An analysis of the dynamical properties of the medium shows, as expected, that small particles move faster than large ones with the self-diffusion coefficients for each species decreasing with the effective crowding. The rate of decrease of the self-diffusion coefficient for tRNAs is 1.3 and 5.6 times greater than those for the ribosomes and proteins, respectively. However, it is to be noted that when the ribosomal charge increases, i.e. when the polydispersity and crowding increase, both tRNAs and ribosomes move less fast than their respective environments, while proteins move faster than their average surroundings. This effect could have important consequences for macromolecular diffusion in the cell. Furthermore, the analysis of the collective diffusion coefficient shows that the combined effects of the polydispersity and of the weak charge of proteins render the system relatively nonrigid as the collective diffusion constant increases relatively little as a function of $\overline{\phi}$.

In this initial study we chose to investigate the simplest system that gave a reasonable representation of the cytoplasm in *E. coli*. Evidently the simulations could be made more realistic,

and several extensions are envisioned. First the interaction potential should be improved by the addition of hydrodynamic terms and a more realistic representation of the electrostatic interactions. The latter, although they are relatively well treated within the DLVO approximation, could be calculated more precisely (by solving the Poisson−Boltzmann equation for example). Second, the size of the cubic box employed in the simulations could be increased and an mRNA molecule added (although this would increase greatly the complexity of the simulations because the mRNA would have to be treated as a chain of particles). Third, a distribution of sizes and charges of proteins could be considered. It may also be possible to treat anisotropic models for the particles and to perform simulations of translational and rotational macromolecular diffusions that are important for association and demixing processes in the mixture. Finally, we hope to compare the results of this and future work more closely with the results that have been obtained from experiment.

Acknowledgment. We thank the reviewers for some useful comments and the Institut de Biologie Structurale−Jean-Pierre Ebel, the Commissariat à l'Energie Atomique, and the Centre National de la Recherche Scientifique for support of this work.

A. Appendix

The virial parameter λ_v appearing in the expression for the collective diffusion constant (eq 26) is defined by

$$\lambda_v = \frac{3}{\langle a^3 \rangle} \sum_{\alpha,\beta} x_\alpha x_\beta \int_0^\infty r^2 [1 - g_{\alpha\beta}(r)]\, dr \qquad (A.1)$$

The calculation of λ_v requires an estimate of the pair distribution functions $g_{\alpha\beta}(r)$. We can write them in terms of the pair potentials of mean force $V_{\alpha\beta}(r)$:

$$g_{\alpha\beta}(r) = \exp\left\{ - \frac{V_{\alpha\beta}(r)}{k_\beta T} \right\} \qquad (A.2)$$

When the particles are weakly charged, the exponential of eq A.2 can be linearized, but for strongly interacting particles a first-order perturbation procedure is used[34] to split $g_{\alpha\beta}(r)$ into reference and perturbation parts:

$$g_{\alpha\beta}(r) = g^0_{\alpha\beta}(r) - g^0_{\alpha\beta}(r) \frac{W_{\alpha\beta}(r)}{k_B T} \qquad (A.3)$$

Here $g^0_{\alpha\beta}(r)$ is the reference hard sphere distribution function defined as

$$g^0_{\alpha\beta}(r) = \begin{cases} 0 & \text{for } r < \sigma'_{\alpha\beta} \\ 1 & \text{for } r \geq \sigma'_{\alpha\beta} \end{cases} \qquad (A.4)$$

and $\sigma'_{\alpha\beta}$ is the rescaled diameter. In the presence of electrostatic interactions the particle radii, a_α, are rescaled to an effective radius a'_α which can be estimated using the procedure described at the beginning of section 3. The pair interaction potential is such that

$$W_{\alpha\beta}(r) = \begin{cases} 0 & \text{for } r < \sigma'_{\alpha\beta} \\ V_{\alpha\beta}(r) & \text{for } r \geq \sigma'_{\alpha\beta} \end{cases} \qquad (A.5)$$

where $V_{\alpha\beta}(r)$ is the DLVO potential described in subsection 2.2. Therefore, we obtain

$$\lambda_v = \frac{1}{\langle (\alpha')^3 \rangle} \sum_{\alpha,\beta} x_\alpha x_\beta \sigma'^3_{\alpha\beta} \left\{ 1 + 3 \frac{\sigma_{\alpha\beta}}{\sigma'_{\alpha\beta}} \frac{V^0_{\alpha\beta}}{k_B T} \frac{[1 + \kappa\sigma'_{\alpha\beta}]}{(\kappa\sigma'_{\alpha\beta})^2} e^{-\kappa\sigma'_{\alpha\beta}} \right\} \qquad (A.6)$$

with

$$V^0_{\alpha\beta} = \frac{Z_\alpha Z_\beta e^2}{\epsilon \sigma_{\alpha\beta}} \left(\frac{e^{\kappa a_\alpha}}{1 + \kappa a_\alpha} \right) \left(\frac{e^{\kappa a_\beta}}{1 + \kappa a_\beta} \right) \qquad (A.7)$$

Note that the second term on the right hand side of eq A.6 describes the nonrescaled part of the electrostatic contribution and is exponentially damped for large $\sigma'_{\alpha\beta}$, i.e. for high charges. In the absence of electrostatic interactions, i.e. when $V^0_{\alpha\beta} = 0$ and $\sigma'_{\alpha\beta} = \sigma_{\alpha\beta} = a_\alpha + a_\beta$, and for small polydispersity, we find the result already obtained by Pusey,[31] namely

$$\lambda_v = \frac{1}{\langle a^3 \rangle} \sum_{\alpha,\beta} x_\alpha x_\beta \sigma^3_{\alpha\beta} \simeq 8 - 12\sigma^2 \qquad (A.8)$$

References and Notes

(1) Goodsell, D. S. *Trends Biochem. Sci.* **1991**, *16*, 203.
(2) Zimmerman, S. B.; Trach, S. O. *J. Mol. Biol.* **1991**, *222*, 599.
(3) Northrup, S. H.; Erickson, H. P. *Proc. Natl. Acad. Sci. USA* **1992**, *89*, 3338.
(4) Einstein, A. *Investigations on the theory of the Brownian movement*; Dover Publications: New York, 1956.
(5) Ackerson, B. J.; Fleishman, L. *J. Chem. Phys.* **1982**, *76*, 2675.
(6) Hanna, S.; Hess, W.; Klein, R. *Physica* **1982**, *A111*, 181.
(7) Felderhof, B. U.; Jones, R. B. *Physica* **1983**, *A121*, 329.
(8) Cichocki, B. *Physica* **1988**, *A148*, 165, 191.
(9) Hess, W.; Klein, R. *Adv. Phys.* **1983**, *32*, 173.
(10) Allison, S. A. *Biophys. J.* **1993**, *65*, 1750.
(11) Northrup, S. H. *Curr. Opin. Struct. Biol.* **1994**, *4*, 269.
(12) Zimmerman, S. B.; Minton, A. P. *Annu. Rev. Biophys. Biomol. Struct.* **1993**, *22*, 27.
(13) Muramatsu, N.; Minton, A. P. *Proc. Natl. Acad. Sci. USA* **1988**, *85*, 2984.
(14) Han, J.; Herzfeld, J. *Biophys. J.* **1993**, *65*, 1155.
(15) Dwyer, J. D.; Bloomfield, V. A. *Biophys. J.* **1993**, *65*, 1810.
(16) Ermak, D. L.; McCammon, J. A. *J. Chem. Phys.* **1978**, *69*, 1352.
(17) Neidhardt, F. C., Ed. *Escherichia Coli and Salmonella Typhimurium: Cellular and Molecular Biology*; American Society for Microbiology: Washington, D.C., 1987; Vols. I and II.
(18) Creighton, T. E. *Proteins: Structures and Molecular Principles*; W. H. Freeman: New York, 1984.
(19) Volkenstein, M. V. *Molecular Biophysics*; Academic Press: New York, 1977.
(20) Tissières, A. *J. Mol. Biol.* **1959**, *1*, 365.
(21) In the paper we define several volume fractions. In general, when we use the term volume fraction without qualification it refers to the volume fraction for a particle or the system calculated with the standard particle radii, a. This is denoted by ϕ_0. The more specific definitions of the other volume fraction terms are defined in the text as they arise.
(22) Cayley, S.; Lewis, B. A.; Guttman, H. J.; Record, M. T., Jr. *J. Mol. Biol.* **1991**, *222*, 281.
(23) Luby-Phelps, K. *Curr. Opin. Cell Biol.* **1994**, *6*, 3.
(24) Medina-Noyola, M. *Phys. Rev. Lett.* **1988**, *60*, 2705.
(25) Hamaker, H. C. *Physica* **1937**, *4*, 1058.
(26) Israelachvili, J. *Intermolecular and Surface Forces*, 2nd ed.; Academic Press: London, 1992.
(27) See as an example of its use in a simulation: Rosenberg, R. O.; Thirumalai, D.; Mountain, R. D. *J. Phys.: Condens. Matter* **1989**, *1*, 2109.
(28) Allen, M. P.; Tildesley, D. J. *Computer Simulations of Liquids*; Oxford University Press: London, 1987.
(29) van Gunsteren, W. F.; Berendsen, H. J. C. *Mol. Simul.* **1988**, *1*, 173.
(30) Mazur, S. *J. Chem. Phys.* **1992**, *97*, 9276.
(31) Pusey, P. N. In *Liquids, Freezing and glass transition II: Les Houches 1989*; Hansen, J. P., Levesque, D., Zinn-Justin, J., Eds.; North-Holland: Amsterdam, 1991.
(32) Schaink, H. M. *Physica* **1994**, *A210*, 113.
(33) See for an example: Riley, D. P.; Oster, G. *Discuss. Faraday Soc.* **1951**, *11*, 107.
(34) Baker, J. A.; Henderson, D. *Rev. Mod. Phys.* **1976**, *48*, 587.

JP9525191